



# CHORUS

This is the accepted manuscript made available via CHORUS. The article has been published as:

## Electronic Transport in Hydrogen-Terminated Si(001) Nanomembranes

Weina Peng, Marziyeh Zamiri, Shelley A. Scott, Francesca Cavallo, James J. Endres, Irena Knezevic, Mark A. Eriksson, and Max G. Lagally

Phys. Rev. Applied **9**, 024037 — Published 28 February 2018

DOI: [10.1103/PhysRevApplied.9.024037](https://doi.org/10.1103/PhysRevApplied.9.024037)

# Electronic Transport in Hydrogen-Terminated Si(001) Nanomembranes

*Weina Peng<sup>‡</sup>, Marziyeh Zamiri,<sup>·</sup> Shelley A. Scott, Francesca Cavallo,<sup>§</sup> James J. Endres, Irena Knezevic, Mark A. Eriksson, and Max G. Lagally*

University of Wisconsin-Madison, Madison, WI 53706, USA

<sup>§</sup>Department of Electrical and Computer Engineering, Center for High Technology Materials,  
University of New Mexico, Albuquerque, NM 87106, USA

Keywords: Si nanomembrane, surface charge transport, H-termination, sheet conductance, surface states.

## Abstract

Charge carrier transport in thin hydrogen (H)-terminated Si(001) sheets is explored via a four-probe device fabricated on silicon-on-insulator (SOI) using the bulk host Si as a back-gate. The method enables electrical measurements without a need to contact the sample surface properly. Sheet conductance measurements as a function of back-gate voltage demonstrate the presence of acceptor and donor-like surface states. These states are distributed throughout the gap and can be

---

<sup>‡</sup> Current address: Micron Technology, 8000 S Federal Way, Boise, ID 83716, USA

<sup>·</sup> Corresponding author: [szamiri@wisc.edu](mailto:szamiri@wisc.edu)

removed or transformed with low-temperature annealing. The density of donor-like states is just under  $10^{12} \text{ cm}^{-2} \text{ eV}^{-1}$  and three times higher than that of the acceptor-like states. We discuss the possible origins of these states. Conductance through the surface layer is too small to measure.

## **Introduction**

In conventional semiconductors, the properties of the charge carriers in the bulk of the material generally dominate the electrical conductance, even though surfaces (or internal interfaces for composite systems) may have their own characteristic conduction properties. As the semiconductor becomes thinner, that is no longer true. The electrical conductance becomes sensitively controlled by an interplay between the electronic structure of the surface(s) and that of the interior of the material (which we shall call “bulk”).<sup>1,2,3,4,5,6</sup> To separate these effects and to identify and potentially enhance the contribution of the surface proper, one can investigate increasingly thin semiconductor sheets, thereby minimizing the possible “bulk” contribution.<sup>1,6,7,8</sup> In materials, such as diamond, in which the bulk conductivity is already very small, it is not necessary to make a very thin sheet,<sup>6</sup> but that is not true for semiconductors in general and Si in particular.

Single-crystal sheets with thicknesses of less than a few 100 nm have come to be called nanomembranes (NMs).<sup>9</sup> Through thinness, extreme flexibility, and a high surface/interface-to-volume ratio, NMs exhibit remarkable mechanical, optical, and electrical properties that are quite different from those of a corresponding bulk crystal. Consequently, NMs have spawned applications in diverse fields, such as flexible and stretchable electronics,<sup>10,11,12,13</sup> photonic structures,<sup>14,15,16</sup> energy storage devices,<sup>17,18</sup> and solar cells.<sup>19</sup> NM structures can be completely free-standing, tethered to a substrate, or bonded to different host materials.<sup>7,20</sup> Obviously, for elec-

tronic applications of NMs or NM/host systems it becomes imperative that the impact of surfaces and interfaces on charge transport be identified and understood.<sup>21,22</sup>

We recently developed an ultra-high-vacuum (UHV) conductance spectroscopy method that generates electrical-transport information in thin semiconductor sheets via back-gate voltage tuning.<sup>23</sup> We utilize a four-probe device fabricated on the semiconductor, along with a back-gate separated from the sample by a dielectric material. This method allows isolation and quantitative determination of the factors that contribute to charge transport in very thin semiconductor sheets. We used this approach to identify and quantify surface charge transport in clean, (2x1) reconstructed Si(001) NMs, by using ever thinner Si sheets to reduce more and more the “bulk” Si contribution to conduction.<sup>23</sup> We showed how surface structure can influence this charge transport, and how the band structure of the “bulk” can interact with that of the surface. We were able to show that the minimum conductance was controlled by the surface, because, as the Si sheet was made thinner, the conductance reached a constant value, as the bulk contribution became smaller and smaller.<sup>23</sup> We also suggested there that the method is broadly applicable.

Here, we extend that work to study the electrical conductance of a similar Si(001) sheet, but with a chemically modified surface, namely a hydrogen termination. As mentioned above, measuring a range of NM thicknesses is critical in order to decouple factors influencing the conductance that relate to the surface/interface from the conductance of the “bulk” Si sheet. In contrast to the results for the clean surface, the minimum sheet conductance here continues to decrease as the Si sheet becomes thinner, implying that we are unable to provide an actual value for the surface conductance. As for the clean surface, however, the shapes of the sheet conductance/back-gate voltage curves provide much information on surface states controlling the charge transport. Analysis of these shapes for Si(001) sheets with H-terminated surfaces demonstrates the pres-

ence of acceptor and donor-like surface states, with the donor-like states dominant by approximately a factor of three, at a density on the order of  $10^{12} \text{ cm}^{-2} \text{ eV}^{-1}$ . They are removed or transformed with low-temperature annealing.

## Experiment

Understanding charge transport in thin semiconductor sheets with chemically modified surfaces is important for the following reasons. In the processing of electronic or optoelectronic devices, the initial surface structure and chemical terminations largely determine subsequent interfacial electronic properties.<sup>24,25,26,27</sup> Additionally, for thin enough materials, surfaces or interfaces may influence the charge transport properties of the entire structure, highlighting the need for both understanding the mechanisms behind surface-bulk interactions and developing new ways to control and tailor these interactions.

Common techniques to examine the surface and interfacial electronic properties and charge transport include conductance-voltage and capacitance-voltage measurements,<sup>28</sup> with surface sensitivity down to  $10^{10} \text{ defects/cm}^{-2} \text{ eV}^{-1}$ .<sup>29</sup> In these methods, however, the required procedures exert a large influence on the surface and underlying interface.<sup>30,31</sup> Consequently, the interpretation of the experimental results is semi-quantitative and sometimes masked by band bending effects at the surface. For that reason, spatially indirect contact for electrical characterization of the surface of thin sheets is extremely appealing.

To characterize the H-terminated Si(001) sheet, we pattern a SiNM into a van der Pauw geometry while it is still bonded to the original host, 3  $\mu\text{m}$  thick  $\text{SiO}_2$  on a Si handle wafer, part of silicon-on-insulator (SOI).<sup>32</sup> The SiNM template layer is p-type (boron doped with nominal doping

level  $\sim 10^{15} \text{ cm}^{-3}$ ) with thickness varying from 77 nm to 220 nm. We create the H termination with a weak-hydrofluoric-acid (HF) dip.

Figure 1(a) shows a schematic diagram of the van der Pauw geometry patterned on SOI and the measurement setup. The device architecture is akin to a pseudo-MOSFET, except that we have a four-probe geometry and vacuum at the front surface. We use the Si handle wafer as a back-gate, which is a key element in our measurements. Details of the fabrication are summarized in the Materials and Methods section and are described in detail in our earlier paper.<sup>23</sup>

Figure 1(b) shows a schematic cross-section of the layer structure, indicating the factors<sup>23</sup> that interact to determine the sheet conductance of the SiNM, including surface states with a density  $D_{it\_surf}$ ; states at the SiNM/BOX interface, with a density  $D_{it}$ ; and fixed oxide charge, with a density  $Q_{ox}$ . In addition, there may be a surface charge,  $Q_{surface}$ . We extract information about these states and their influence on charge transport in the SiNM through measurement of the sheet conductance as a function of back-gate voltage and modeling to fit the experimental results.

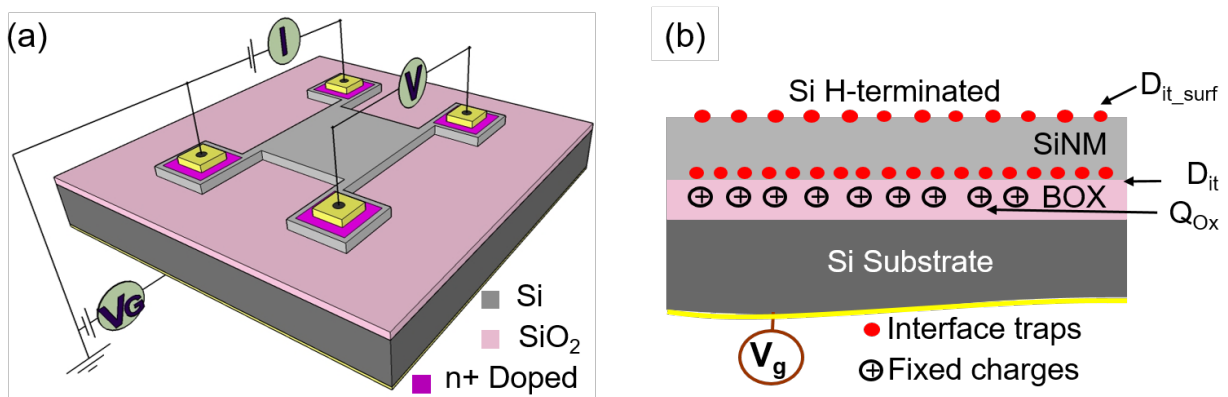


**Figure 1.** Schematic diagram of the van der Pauw measurement on Si NMs and a cross section of the device. (a) A mesa is patterned on the SOI wafer, representing an inverted MOSFET structure. The central region is  $4 \times 4 \text{ mm}^2$ ; the four corner contacts are doped with P. One of eight possible measurements is shown in the diagram, with current passing through two adjacent contacts and voltage measured between the other two. The Si substrate serves as a back-gate. (b) Schematic cross-sectional view of H-terminated SOI(001), showing localized states, as described in the text.

## **Materials and methods**

*Device fabrication.* The sheet conductance method employs a four-probe, van der Pauw configuration geometry fabricated on SiNMs bonded on their original host substrate, silicon-on-insulator (SOI),<sup>32</sup> as shown in Fig. 1(a). The nominal doping of the substrate is p-type  $N_A \sim 10^{15} \text{ cm}^{-3}$ . In essence, a mesa is patterned with four contacts pads, and the surrounding Si removed to isolate the structure. The pads are then doped to ensure ohmic contact with the 4 metal sample holder pressure clamps that are used to inject current and measure the voltage through the sample. Before introduction to the UHV system, the surface is thoroughly degreased with acetone and isopropanol, followed by 15 min UV ozone, and then chemically cleaned using standard RCA (Radio Corporation of America)<sup>33</sup> procedures before a final HF dip (10% HF, 20s) to terminate it with hydrogen. Immediately after, the sample is mounted and transferred to the measurement chamber, where spring loaded connectors attach to the sample holder clamps. All contacts are grounded throughout sample installation to prevent electrostatic shock, which is detrimental to the buried oxide layer. The procedure is required to avoid oxide leakage current. A base pressure of  $< 1 \times 10^{-10}$  Torr enables stable and repeatable measurements. Different membrane thicknesses are obtained by thinning the SOI prior to device fabrication. An initial 220nm SOI wafer is thinned with repeated oxidation at 1150C, followed by oxide stripping in HF.

*Theory.* Surface electrical information is obtained from comparisons between experimental results and numerical simulations. The entire SOI system is treated as a gate-insulator-semiconductor capacitor (from substrate towards the surface). The band diagram is constructed by solving Poisson's equation throughout the system. The membrane sheet conductance is then calculated from

the local carrier concentration. In this way,  $G$  is obtained as a function of  $V_g$ . A detailed description of the model can be found in the Supplemental Material<sup>34</sup> and in ref.35.<sup>35</sup>

*Measurement System.* Ultra-high vacuum (UHV) provides excellent control of sample surfaces, and is crucial to the stabilization of measurement conditions. From a load lock at  $\sim 10^{-8}$  Torr, a mechanical arm pushes the sample holder into the main chamber, whose base pressure is  $\sim 8 \times 10^{-11}$  Torr.

The sample is heated radiatively or by electron bombardment with a tungsten filament behind the sample. Radiative heating alone is used for annealing at low temperature.

*X-ray photoelectron spectroscopy.* XPS was performed primarily with a PHI 5600 ESCA system with a monochromatic Al  $K\alpha$  source ( $h\nu = 1486.6$  eV). The Supplemental Material provides more details.<sup>34</sup>

*Electrical measurements.* We make eight four-probe measurements for each back-gate voltage, from which we deduce the conductance per square using the standard van der Pauw formulas.<sup>36</sup> By using the van der Pauw analysis, we implicitly assume the template layer is thin enough (220 nm or less) compared with its lateral dimensions ( $4 \times 4$  mm<sup>2</sup>) that equilibrium between the front and the back interfaces is achieved over lateral length scales much smaller than the device dimensions.<sup>23</sup> Furthermore, the  $4 \times 4$  mm<sup>2</sup> central device mesa is defined by etching down to the buried oxide. The mesa reaches the contact regions via four 500  $\mu$ m wide and 500  $\mu$ m long arms. This geometry causes less than 1% experimental error in van der Pauw sheet resistance measurements.

## **Results and Discussion**

To measure the sheet conductance we sweep the back-gate voltage,  $V_g$ , from high positive to high negative values. Figure 2(a) shows a representative sheet conductance- $V_g$  curve with the regions of interest highlighted (see figure caption). As we sweep to more negative back-gate voltage, holes accumulate at the internal oxide/SiNM interface, eventually forming an accumulation channel, with the flat band voltage ( $V_{FB}$ ) defined by the onset of this channel. A schematic band diagram representative of this condition is shown in the top left of the plot. Similarly, as we sweep to positive  $V_g$ , electrons accumulate in the SiNM at the oxide/NM interface to form an inversion channel, with the threshold voltage,  $V_T$ , defining the onset. It is the region between the flat-band and threshold voltages that yields critical information on the electronic behavior of the NM.<sup>23, 37</sup>

Fig 2(b) shows log sheet conductance- $V_g$  curves of H-terminated SiNMs having thicknesses of 77 nm, 120 nm, and 220 nm. All NMs show both hole accumulation and electron inversion regions when the gate voltage is highly negative or highly positive respectively, with clear ambipolar behavior (both electron and hole conduction). Between these regions, the NM conductance reaches a minimum ( $G_{min}$ ). Moreover, the conductance-voltage curve has a distinctly asymmetric shape, with an obvious change of curvature on the positive-voltage side. The  $G_{min}$  value drops by more than one order of magnitude as the membrane thickness decreases from 220 to 77 nm. In addition, the conductance minimum is broader for thinner NMs.

As indicated above and illustrated schematically in Fig. 1(b), the various localized states at the surface and interfaces will influence the conductance-voltage characteristics of this type of structure. In addition, the NM “bulk” will contribute to the sheet conductance. The nominal doping level (here  $N_A \sim 10^{15} \text{ cm}^{-3}$ ), and the thickness of the NM control this contribution. We deliberately use a thin sheet to lower this contribution. For this doping density and the range of NM thick-

nesses used here, the total number of dopants contained in the NM is  $10^9 - 10^{10} \text{ cm}^{-2}$ , depending on the NM thickness. As we show next, the combination of low  $N_A$  and thinness diminishes the effect of bulk doping on the conductance, allowing any influence caused by the surface termination to become observable.<sup>23</sup>

Figure 2(c) shows the minimum sheet conductance of the “bulk” of the NM calculated for three different NM thicknesses and compares it to the measured values (the minima shown in Fig. 2(b)). To calculate this sheet conductance we use:

$$G_{min}(bulk) = qt(\mu_h n_h + \mu_e n_e), \quad (1)$$

where  $q$  is electronic charge,  $t$  is NM thickness,  $\mu_e$  is electron mobility,  $n_e$  is electron density,  $\mu_h$  is hole mobility, and  $n_h$  is hole density. For this calculation, we assume that the NM “bulk” dopants alone determine the minimum sheet conductance of a thin NM; i.e., there is no effect of surface and interface. As the NM is p-doped,  $\mu_h n_h$  has the dominant role in this “bulk” sheet conductance. Using Eq. (1) we calculate for p-doped NMs ( $n_p=10^{15} \text{ cm}^{-3}$ ) with thicknesses of 77 nm, 120 nm, and 220 nm sheet conductances of  $6.8 \times 10^{-7} \Omega^{-1} \square^{-1}$ ,  $1.1 \times 10^{-6} \Omega^{-1} \square^{-1}$ , and  $1.9 \times 10^{-6} \Omega^{-1} \square^{-1}$ , respectively. The decrease of  $G_{min}$  with thickness for the “bulk” is linear, as it is proportional to the volume, which decreases linearly with decreasing thickness.

The measured values, also shown in Fig. 2(c), of the sheet conductance at the value of  $V_g$  corresponding to  $G_{min}$  are several orders of magnitude lower than the  $G_{min}$  value calculated for the “bulk” component at corresponding thicknesses, thus demonstrating the dominant influence of the chemically modified surface and states associated with it. The measured minimum sheet conductance values do not decrease linearly with reduced thickness, [ $2 \times 10^{-9} \Omega^{-1} \square^{-1}$  for 220nm,

$3.9 \times 10^{-10} \Omega^{-1} \square^{-1}$  for 120nm, and  $1.1 \times 10^{-10} \Omega^{-1} \square^{-1}$  for 77nm]. The thickness of the NM does determine the coupling strength between the front H-terminated surface and the back-gate, via modification of the membrane capacitance. Thinner membranes have a higher capacitance and therefore the effects at the surface exert a stronger influence on the conduction properties.

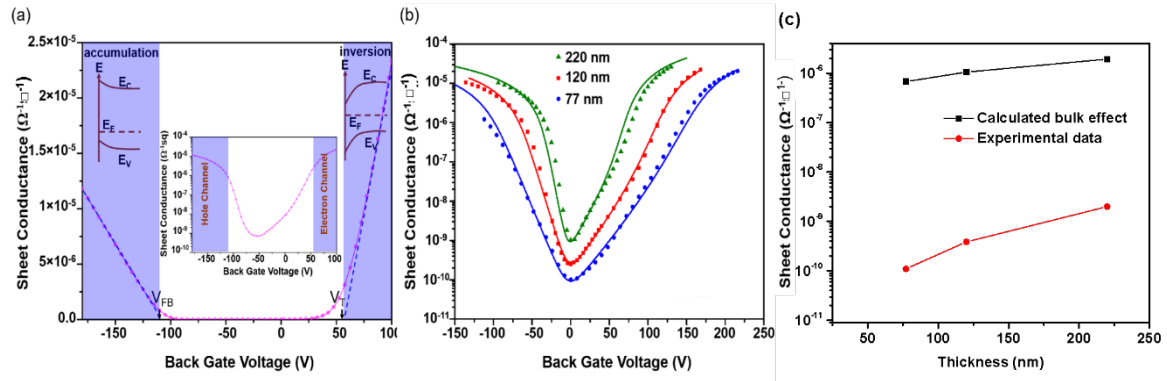


**Figure 2.** Sheet conductance as a function of back-gate voltage for H-terminated SOI(001). (a) Graph for a 120 nm thick Si template layer. The data are plotted in linear and log (inset) scales. The flat-band voltage  $V_{FB}$  and the threshold voltage  $V_T$  are extracted from linear extrapolations of the curve at high negative and positive gate voltages respectively. Surface and interface-related electrical information is determined from the low-conductance region (white region, between  $V_{FB}$  and  $V_T$ ). The insets show the band diagrams at the oxide/NM interface. Figure adapted from Ref. 23. (b) Data (symbols) and simulation fits (lines) of conductance-voltage measurements on H-terminated SOI(001) for three different Si template thicknesses: 77 nm, 120 nm, and 220 nm. The curves are shifted along the voltage axis to have the sheet conductance minima appear at zero back-gate voltage. Uncertainties in the NM thickness and the electrical measurements are sufficiently small that the resulting uncertainty in the sheet conductance does not exceed the size of the data points shown in (b). (c) Comparison between the naïve calculated minimum conductance, as described in the text, of the NM “bulk” and experimental data (containing both bulk and surface effects) for  $G_{min}$ , shown in (b) for 77 nm, 120 nm, and 220 nm thick SiNMs.

Previous studies on pseudo-MOSFETs<sup>21,22</sup> have shown that states at the interface of the Si template layer and the buried oxide trap charge and thus affect the subthreshold slope via  $1/C_{ox}$ , where  $C_{ox}$  is the oxide capacitance ( $C_{ox} = \epsilon_{ox}/t_{ox}$ , approximately  $1 \text{ nF/cm}^2$ ). States at the top Si surface affect the slope via a more complex term,  $\frac{1}{C_{ox}} \times \frac{C_{Si}}{C_{Si} + C_{it\_Si\_H}}$ . Here  $C_{Si}$  is the membrane ca-

capacitance ( $C_{Si} = \epsilon_{Si}/t_{Si}$ , about 50 nF/cm<sup>2</sup> for a 220 nm thick NM and 140 nF/cm<sup>2</sup> for a 77 nm thick NM) and  $C_{it\_Si-H}$  is the interface state capacitance of H-terminated Si ( $C_{it\_Si-H} = q^2 D_{it\_Si-H}$ , about 160 nF/cm<sup>2</sup> for  $D_{it} = 10^{12}$  cm<sup>-2</sup>eV<sup>-1</sup>). For our thin NMs the latter term roughly equals 0.24 and 0.47 of the  $I/C_{ox}$  at the Si/SiO<sub>2</sub> interface for 220 nm and 77 nm thick SiNMs, respectively. The H-terminated surface therefore should have an important influence on the carrier transport within the NM. A thinner membrane has a larger  $C_{Si}$ , thus a stronger coupling strength between the H-terminated Si surface and the back-gate, and a stronger effect of this surface on the NM conductance.

Figure 2(b) also shows fits to the data, using a model<sup>23,28,35</sup> that includes both fixed oxide charges ( $Q_{ox}$ ) and interface states ( $D_{it\_ox}$ ) at the Si template layer/SiO<sub>2</sub> interface. The positive fixed oxide charges are located on the SiO<sub>2</sub> side, within 3 nm from the interface.<sup>38</sup> The energies of the interface states are uniformly distributed across the Si band gap, with acceptor-like states above and donor-like states below the center of the bandgap.<sup>28</sup> By definition, donor-like states are neutral when occupied by electrons and positively charged when empty, while acceptor-like ones are negatively charged when occupied and neutral when empty. For H-terminated Si(001), the model, fully described in Ref. 35, assumes that donor-like states ( $D_{it\_Hdonor}$ ) and acceptor-like states ( $D_{it\_Hacceptor}$ ) coexist, but in different amounts. For simplicity, we also assume that both types of these NM surface states have a uniform energetic distribution throughout the band gap. This assumption is equivalent to a picture in which the neutrality point lies away from the center of the Si band gap. This model captures the main aspects of the surface electronic structure with the fewest number of fitting parameters.<sup>23,28,35</sup> A schematic diagram of our one-dimensional simulation model<sup>23, 35</sup> is shown in Fig. 1(b). Using the four parameters  $D_{it\_ox}$ ,  $D_{it\_Hdonor}$ ,  $D_{it\_Hacceptor}$ , and  $Q_{ox}$  and setting up the corresponding boundary conditions, we solve 1D Poisson's equations nu-

merically, extracting the local potential as well as the carrier concentrations as a function of the depth into the SiNM. The membrane conductance is then calculated from the carrier concentration and the electron and hole mobilities, taking into consideration the mobility degradation caused by phonons, dopants, and above all interface roughness (See Supplemental Material for more details<sup>34</sup>). The simulated conductance- $V_g$  curves agree well with the data. The fitting parameters used for the three thicknesses are consistent with each other, suggesting the simple model we are using describes the actual system quite well.

Table 1 shows these fitting parameters and demonstrates that we can quantitatively determine state densities. In particular, there is a large population of localized trap states on H-terminated Si(100) surfaces, and the majority of these trap states are donor-like. The approximately 3 times as many donor-like states as acceptor-like ones leads directly to the asymmetric conductance-voltage curve. The opposite situation, i.e., a majority of acceptor-like states, would lead to a curve shape in contradiction to what is observed in Fig. 2 (b). (See Fig. S2 in the Supplemental Material.<sup>34</sup>) Table 1 also shows that all fitting parameters become slightly larger as the NM becomes thinner. All values, except for  $Q_{ox}$ , are within a factor of two for the different thicknesses. We may be able to attribute the increase in  $D_{it\_ox}$  and  $Q_{ox}$  to additional cycles of thermal oxidation at high temperature (1050°C) followed by oxide removal in HF in order to reach the desired NM thicknesses.  $Q_{ox}$  in any case only affects the value of  $V_g$  at which  $G_{min}$  occurs. The small increases in surface state densities as the NM gets thinner may be associated with surface roughness induced by multiple exposures of the surface to HF during the thinning process.

**Table 1.** Fitting parameters used for the simulation curves shown in Fig. 1(b).  $D_{it\_ox}$  and  $Q_{ox}$  represent the interface state density and the fixed oxide charge at the Si/SiO<sub>2</sub> interface, respectively.  $D_{it\_Hdonor}$  and  $D_{it\_Hacceptor}$  are donor-like and acceptor-like surface states at the H-terminated Si(100) surface. The values have an uncertainty from 3 to 9 percent.

Membrane Thickness (nm)	$D_{it\_ox}$ ( $cm^{-2} eV^{-1}$ )	$Q_{ox}$ ( $cm^{-2}$ )	$D_{it\_Hdonor}$ ( $cm^{-2} eV^{-1}$ )	$D_{it\_Hacceptor}$ ( $cm^{-2} eV^{-1}$ )
220	$8.7 \times 10^{11}$	$1.0 \times 10^{10}$	$6.7 \times 10^{11}$	$2.3 \times 10^{11}$
120	$1.4 \times 10^{12}$	$1.0 \times 10^{10}$	$8.1 \times 10^{11}$	$2.9 \times 10^{11}$
77	$1.9 \times 10^{12}$	$2.7 \times 10^{11}$	$9.3 \times 10^{11}$	$3.3 \times 10^{11}$

To explain the sheet conductance-voltage results, and to understand the influence of these donor-like states on the carrier transport in SiNMs, it is useful to investigate the band bending in a SiNM at different back-gate voltages. The simulated band diagrams at three different conditions are examined in Fig. 3 for a 77 nm thick SiNM: at accumulation (Fig. 3(b)), at the conductance minimum  $G_{min}$  (Fig. 3(c)), and at inversion (Fig. 3(d)), which are marked with red circles on the sheet conductance - gate voltage curve shown in Fig. 3(a). The data of Fig 3(a) were already shown as part of Fig. 2(b), but here  $G_{min}$  appears at a negative gate voltage, because the minimum has not been shifted to zero gate voltage, as it was in Fig 2(b) to enhance comparison. The positive fixed oxide charge at the template Si/SiO<sub>2</sub> interface and a large number of unoccupied donor-like states (positively charged) at the H-terminated Si(100) surface act effectively as a gate voltage to shift  $G_{min}$ .

At  $V_g = -250V$ , as expected, the Fermi level is very close to the valence band edge at the back template Si/SiO<sub>2</sub> interface and holes accumulate at the interface, near the oxide. However, the Fermi level is pinned near midgap for H-terminated Si(001) surfaces, because of the large number of donor states at the surface. Above the surface Fermi level,  $E_{Fs}$ , those donor-like states are unoccupied and thus positively charged. As a result, there exists a large band bending within the membrane, with the electric field pointing from the Si-H surface to the SiNM/buried-oxide interface. When the back-gate voltage is increased, the Fermi level moves up correspondingly. The

change in position of  $E_{Fs}$ , the Fermi level at the H-terminated Si(001) surface, is considerably less than it is at the Si/SiO<sub>2</sub> interface, with  $E_{Fs}$  remaining near the midgap. Moreover, the band bending across the membrane, as well as the number of surface positive charges, is slightly reduced, Fig. 3(c). The conductance reaches its minimum value when  $E_{Fs}$  intersects  $E_i$  ( $V_g = -96$  V, Fig. 3(a)). The thickness comes into play because the carrier concentration in the membrane per unit area is proportional to the thickness. At this voltage, the total carrier concentration within the membrane is as small as it can be, and the numbers of electrons and holes are approximately equal. When  $V_g$  is further increased to more positive voltages, the conductance increases again as  $E_{Fs}$  moves closer to the conduction band, Fig. 3(d). Finally, the whole membrane becomes inverted (for this 77nm NM, at  $V_g = 96$  V). Most of the donor-like states at the H-terminated Si(100) surface are now filled, and so are the acceptor-like states. This fact gives rise to the slightly negatively charged H-terminated Si surface at this condition, and the relatively flat bands in the SiNM.

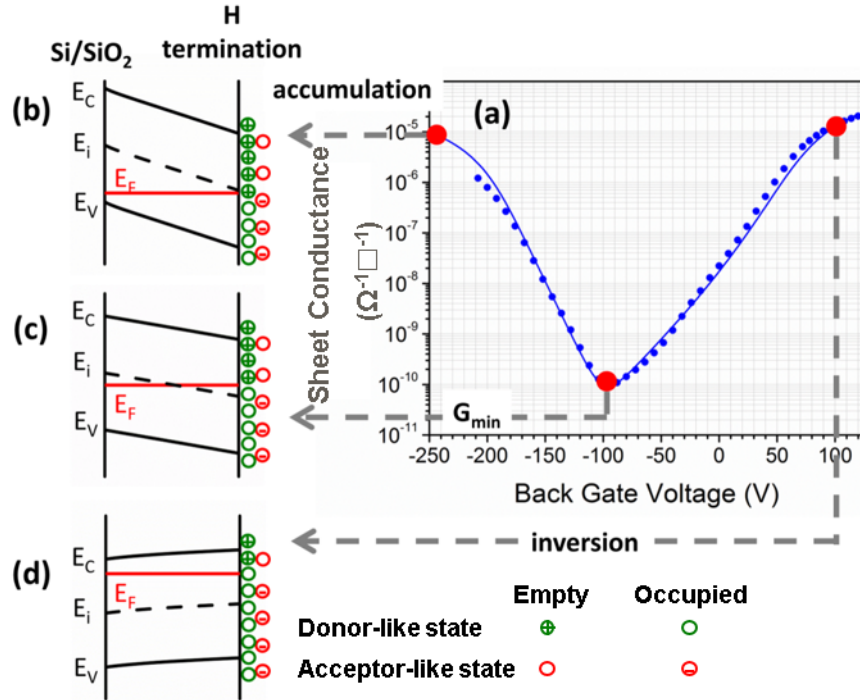


**Figure 3.** Diagrams for bands at three back-gate voltage conditions for a H-terminated Si(001)NM. (a) The sheet conductance-voltage curve for a 77 nm thick SiNM. Unlike the curves presented in Figure 2(b), the curve here is not shifted along the voltage axis. (b), (c) and (d) are simulated diagrams of the positions of bands and the Fermi level across the SiNM at three different voltages:  $V_g = -250$  V (accumulation),  $V_g = -96$  V (at conductance minimum) and  $V_g = 96$  V (inversion). Experimental  $V_g$  values are obtained from -210 V to 120 V, limited by the range of the voltage source. For simplicity the only band bending shown in these diagrams is due to back-gate voltage.

The simulation demonstrates that the position of  $E_{FS}$  at the H-terminated Si surface can be varied under the influence of a back-gate. For most of the range of gate voltages, H-terminated Si(100) has a net positive surface charge because of the unoccupied donor states; therefore, a large electric field is established across the membrane. The position of the Fermi level at the surface has a limited range (from approximately the midgap to near the conduction band edge for a 77 nm thick NM) under the influence of the back-gate. This range is reduced for a thicker membrane (see Supplemental Material<sup>34</sup> for simulations on 220 nm thick NMs, Fig. S3). Consequently, fewer surface electrical defects are probed, resulting in a narrower shape of the sheet conduct-

ance curve for thicker NMs, as is evident in Fig. 2(b). Around  $G_{min}$ , the band bending in NMs of different thicknesses is approximately the same. Also, those surface states on H-terminated Si(100) that are below the midgap cannot be detected even for the thinnest NM used in our experiment. This conclusion will not change even when we change the substrate doping from low  $p$  type to low  $n$  type, as the bulk dopants are completely irrelevant here. The only way to increase the probing range is to use a thinner membrane, which increases the membrane capacitance  $C_{Si}$ , and therefore the coupling strength between the back-gate and the top surface. An extremely thin SiNM (below 10 nm), may enable characterization of the states in the H-terminated surface within the entire Si band gap.

Our back-gated four-probe measurements, in conjunction with simulations, allow us to extract quantitative information on the role interface states play in the electronic-transport properties of thin semiconductors or surfaces.

We now consider the origin of the donor-like states at the H-terminated Si(001) surface. It is known that this surface is atomically disordered, with dihydrides as the dominant surface species.<sup>39</sup> Prior measurements, using spectroscopic methods, found a large band bending on bulk Si(100) surfaces after HF treatment<sup>40,41,42</sup> for various doping levels and types. As shown in Fig. 3(a), NMs are under weak inversion when no gate voltage is applied, because of these unoccupied donor-like surface states. They constrain the movement of the surface Fermi level during sweeps of the gate voltage until the membrane is strongly inverted, equivalent to highly  $n$ -doped bulk Si (which is the one doping type that did not produce the band bending suggestive of donor-like surface states<sup>40</sup>). Our simulation shows that positive fixed oxide charges, which are located at the template Si/buried-oxide interface, are one order of magnitude lower in density than

$D_{it\_Hdonor}$  and thus play a minor role. With back-gate tuning, the effective carrier density in the NM is efficiently changed.

Although we identify surface states as unoccupied, donor-like states, their origin is uncertain. Residual species such as OH and fluorine groups are often detected on H-terminated Si(100) after HF etching, and their amount depends on the HF concentration and the following rinse time (when it occurs) in DI water. XPS studies of the as-prepared H-terminated Si(100) surfaces frequently show traces of O and C but no F signal [see Supplemental Material<sup>34</sup>]. In any case, as both oxygen and fluorine are more electronegative than Si, they will not donate electrons to Si and become positively charged. Some studies suggest the very initial attack of the H termination by humidity as a cause of the large band bending observed on Si-H terminations.<sup>43</sup>

There appear to be two possibilities to explain our measurements: 1) adventitious contamination on the HF treated surfaces that is introduced via the HF or via the ambient in the time between removal of the sample from the bath and introduction to the UHV system. Because of the low density of states relative to a monolayer, a concentration of contaminants far below the detection limit of XPS is needed. 2) Disordered adsorbed H, rather than contamination. To search for further understanding, we annealed the H-terminated sample, by radiatively heating it via a filament from the back. The annealing temperature is low enough ( $\sim 270^\circ\text{C}$ ) not to desorb any hydrogen<sup>44</sup> or affect the properties of the buried-oxide interface, but adventitious contamination that is weakly bound to the surface could be removed. Additionally disordered H could rearrange on the surface into better order. With a short  $270^\circ\text{C}$  anneal the sheet conductance curve changes dramatically. The minimum in the curve shifts to more positive gate voltages and the curve itself becomes distinctly narrower and more symmetric, as is shown in Fig. 4. A sharp  $1\times 1$  LEED pattern

appears after the anneal, while no LEED pattern can be observed on as-prepared H-terminated surface. This behavior is also frequently observed in STM studies of the H/Si surface.<sup>43</sup>

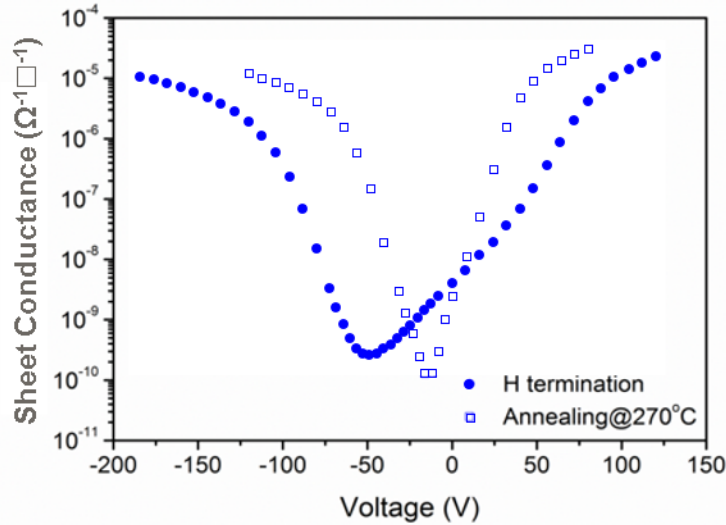


**Figure 4.** Measured sheet conductance-voltage curves of a 77 nm thick H-terminated SiNM before and after short-time, low-temperature annealing at 270°C.

One can explain the drastic change in the sheet conductance-voltage curve by the removal of donor-like states. Fig. 4 shows that the left part of the G-V curve stays almost the same. It is known from our simulation that this part is mainly determined by the Si/SiO<sub>2</sub> interface, suggesting no change happens at the buried-oxide interface. On the other hand, the right part of the conductance-voltage curve becomes much steeper after the annealing, indicating a decrease of total number of defects. Obviously, the decrease of localized states must come from the top surface. Because the curve shifts to more positive voltages after the annealing, the change in surface charge is thus of positive sign, pointing to donor like states. The decrease in  $D_{it\_H-donor}$  unpins the surface Fermi level and the characteristic asymmetric G-V curve due to the imbalance between acceptor and donor states disappears.

These observations alone cannot distinguish between removal of adventitious adsorbates or ordering of H on the surface when the surface is annealed. Nor can the sharpening of the LEED

pattern, or the ability to see STM images after annealing, distinguish between these choices. However, the following might bias the conclusion in one direction. We have the ability to dose the surface in situ with monatomic H. A clean surface dosed with H assumes the broad shape of the conductance curves for the original HF terminated surface.<sup>45,46</sup> Thus disordered clean, atomic H can have the same effect as a HF treatment. We therefore favor a conclusion that the states that low-temperature annealing removes appear to be caused by very loosely bound (e.g., physisorbed) or easily transformable H species.

## **Conclusion**

We have characterized H-terminated Si(001) surfaces using a contactless NM conductance method.<sup>23</sup> The contribution that this method makes to the general problem of surface states on clean or chemically modified surfaces is the ability to identify different states and quantify their relative contributions, as fits to the sheet conductance - voltage curves are extremely sensitive to the nature and density of the states. For H-terminated Si(001), donor-like states, at a density in the high  $10^{11} \text{ cm}^{-2} \text{ eV}^{-1}$  range, are found to exist on the surface. Low-temperature annealing easily removes or transforms these states. Their origin is uncertain, as explained above. The simplest explanation would be that adventitious contamination is removed with a soft anneal; however, dosing a clean surface with atomic H in situ produces quite similar conductance curves as found for HF terminated surfaces.<sup>45,46</sup>

The use of very thin sheets and back-gated van der Pauw measurements described here can readily be applied to other surface terminations and other semiconductor systems. For semiconductor surfaces other than Si, the influence of surface chemistry on charge transport is even less well known. For example in III-V semiconductors, surface terminations that significantly lower

the surface defect density would largely improve the technological development of III-V semiconductors. Accurate surface electrical characterization will also benefit the development of semiconductor surface passivation chemistries.

### **Corresponding Author**

\*Marziyeh Zamiri, Email: [szamiri@wisc.edu](mailto:szamiri@wisc.edu)

### **Author Contributions**

W.P. performed experiments under the guidance of M.A.E. and M.G.L. J. J. E. and I.K. provided theoretical support. W.P., S.A.S., M.Z. and F.C. analyzed the data. All authors participated in writing the manuscript.

### **Notes**

The authors declare no competing financial interest.

### **Acknowledgments**

This research was primarily supported by the U.S. Department of Energy (DOE), Office of Science, Basic Energy Sciences (DOE BES) Award #DEFG02-03ER46028. We acknowledge the use of facilities and instrumentation supported by NSF through the University of Wisconsin Materials Research Science and Engineering Center, DMR-1121288. IK acknowledges support by the DOE BES Award #DE-SC0008712. The work of W.P. was partially supported by NSF. The work of J.J.E. was supported by a Blue Waters Undergraduate Petascale Research Internship through the Blue Waters Project at the National Centre for Supercomputing Applications and funded by the NSF Office of Cyber Infrastructure. Finally, we would like to thank the one anon-

ymous reviewer who expended extraordinary effort in assessing our writing and thereby caused us to improve the MS significantly.

## References

---

- [1] P. Zhang, E. Tevaarwerk, B. N. Park, D. E. Savage, G. K. Celler, I. Knezevic, P. G. Evans, M. A. Eriksson, and M. G. Lagally, Electronic Transport in Nanometre-Scale Silicon-on-Insulator Membranes, *Nature* **439**, 703 (2006).
- [2] Y. Cui, Q. Wei, H. Park, and C. M. Lieber, Nanowire Nanosensors for Highly Sensitive and Selective Detection of Biological and Chemical Species, *Science* **293**, 1289 (2001).
- [3] Y. Pan, Y. Tao, G. Qin, Y. Fedoryshyn, S. N. Raja, M. Hu, C. L. Degen, and D. Poulikakos, Surface Chemical Tuning of Phonon and Electron Transport in Free-Standing Silicon Nanowire Arrays, *Nano Letters* **16**, 6364 (2016).
- [4] T. He, J. He, M. Lu, B. Chen, H. Pang, W. F. Reus, W. M. Nolte, D. P. Nackashi, P. D. Franzon, and J. M. Tour, Controlled Modulation of Conductance in Silicon Devices by Molecular Monolayers. *Journal of the American Chemical Society* **128**, 14537 (2006).
- [5] J. J. Boland, Semiconductor Physics: Transport News, *Nature* **439**, 671 (2006).
- [6] J. Ristein, Surface Transfer Doping of Semiconductors, *Science* **313**, 1057 (2006).
- [7] S. A. Scott, W. Peng, A. M. Kiefer, H. Jiang, I. Knezevic, D. E. Savage, M. A. Eriksson, and M. G. Lagally, Influence of Surface Chemical Modification on Charge Transport Properties in Ultrathin Silicon Membranes, *ACS Nano* **3**, 1683 (2009).
- [8] M. Zhou, Z. Liu, Z. Wang, Z. Bai, Y. Feng, M. G. Lagally, and F. Liu, Strain-Engineered Surface Transport in Si (001): Complete Isolation of the Surface State via Tensile Strain, *Physical Review Letters* **111**, 246801 (2013).

- 
- [9] F. Cavallo, and M. G. Lagally, Semiconductors Turn Soft: Inorganic Nanomembranes, *Soft Matter* **6**, 439 (2010).
- [10] D. Y. Khang, H. Jiang, Y. Huang, and J. A. Rogers, A Stretchable Form of Single-Crystal Silicon for High-Performance Electronics on Rubber Substrates, *Science* **311**, 208 (2006).
- [11] H. C. Ko, M. P. Stoykovich, J. Song, V. Malyarchuk, W. M. Choi, C. J. Yu, J. B. Geddes Iii, J. Xiao, S. Wang, Y. Huang, J. A. Rogers, A Hemispherical Electronic Eye Camera Based on Compressible Silicon Optoelectronics. *Nature* **454**, 748 (2008).
- [12] L. Sun, G. Qin, J. H. Seo, G. K. Celler, W. Zhou, and Z. Ma, 12-GHz Thin-Film Transistors on Transferrable Silicon Nanomembranes for High-Performance Flexible Electronics, *Small* **6**, 2553 (2010).
- [13] R. H. Kim, D. H. Kim, J. Xiao, B. H. Kim, S. I. Park, B. Panilaitis, R. Ghaffari, J. Yao, M. Li, Z. Liu, V. Malyarchuk, D. G. Kim, A. P. Le, R. G. Nuzzo, D. L. Kaplan, F. G. Omenetto, Y. Huang, Z. Kang, and J. A. Rogers, Waterproof AlInGaP Optoelectronics on Stretchable Substrates with Applications in Biomedicine and Robotics, *Nature Materials* **9**, 929 (2010).
- [14] H. Yang, D. Zhao, S. Liu, Y. Liu, J. H. Seo, Z. Ma, and W. Zhou, Transfer Printed Nanomembranes for Heterogeneously Integrated Membrane Photonics, *Photonics* **2** 1081 (2015).
- [15] P. Feng, G. Wu, O. G. Schmidt, and Y. Mei, Photosensitive Hole Transport in Schottky-Contacted Si Nanomembranes, *Applied Physics Letters* **105**,121101 (2014).
- [16] X. Xu, H. Subbaraman, D. Kwong, A. Hosseini, Y. Zhang, and R. T. Chen, Large Area Silicon Nanomembrane Photonic Devices on Unconventional Substrates, *IEEE Photonics Technology Letters* **25**, 1601 (2013).

- 
- [17] C. C. Bufon, J. D. Cojal Gonzalez, D. J. Thurmer, D. Grimm, M. Bauer, and O. G. Schmidt, Self-Assembled Ultra-Compact Energy Storage Elements Based on Hybrid Nanomembranes, *Nano Letters* **10**, 2506 (2010).
- [18] H. X. Ji, X. L. Wu, L. Z. Fan, C. Krien, I. Fiering, Y. G. Guo, Y. Mei, and O. G. Schmidt, Self-Wound Composite Nanomembranes as Electrode Materials for Lithium Ion Batteries, *Advanced Materials* **22**, 4591 (2010).
- [19] J. Lee, J. Wu, M. Shi, J. Yoon, S. I. Park, M. Li, Z. Liu, Y. Huang, and J. A. Rogers, Stretchable GaAs Photovoltaics with Designs that Enable High Areal Coverage, *Advanced Materials* **23**, 986 (2011).
- [20] Y. Zhang, F. Zhang, Z. Yan, Q. Ma, X. Li, Y. Huang, and J. A. Rogers, Printing, Folding and Assembly Methods for Forming 3D Mesostructures in Advanced Materials, *Nature Reviews Materials* **2**, 17019 (2017).
- [21] N. Rodriguez, S. Cristoloveanu, and F. Gamiz, Revisited Pseudo-MOSFET Models for the Characterization of Ultrathin SOI Wafers, *IEEE Transactions on Electron Devices* **56**, 1507 (2009).
- [22] S. Cristoloveanu, D. Munteanu, and M. S. Liu, A Review of the Pseudo-MOS Transistor in SOI Wafers: Operation, Parameter Extraction, and Applications, *IEEE Transactions on Electron Devices* **47**, 1018 (2000).
- [23] W. Peng, Z. Aksamija, S. A. Scott, J. J. Endres, D. E. Savage, I. Knezevic, M. A. Eriksson, and M. G. Lagally, Probing the Electronic Structure at Semiconductor Surfaces Using Charge Transport in Nanomembranes, *Nature Comm.* **4**, 1339 (2013).

- 
- [24] T. Takahagi, I. Nagai, A. Ishitani, H. Kuroda, and Y. Nagasawa, The Formation of Hydrogen Passivated Silicon Single-Crystal Surfaces Using Ultraviolet Cleaning and HF Etching, *J. Appl. Physics* **64**, 3516 (1988).
- [25] M. R. Linford, and C. E. Chidsey, Alkyl Monolayers Covalently Bonded to Silicon Surfaces, *J. the American Chemical Society* **115**, 12631 (1993).
- [26] J. Terry, M. R. Linford, C. Wigren, R. Cao, P. Pianetta, and C. E. Chidsey, Determination of the Bonding of Alkyl Monolayers to the Si(111) Surface Using Chemical-Shift, Scanned-Energy Photoelectron Diffraction, *Appl. Phys. Lett.* **71**, 1056 (1997).
- [27] W. Peng, W. J. DeBenedetti, S. Kim, M. A. Hines, and Y. J. Chabal, Lowering the Density of Electronic Defects on Organic-Functionalized Si(100) Surfaces, *Appl. Phys. Lett.* **104**, 241601 (2014).
- [28] T. Ando, A. B. Fowler, and F. Stern, Electronic Properties of Two-Dimensional Systems, *Reviews of Modern Physics* **54**, 437 (1985).
- [29] S. M. Sze, *Physics of Semiconductor Devices*, John Wiley & Sons 1981.
- [30] E. Yablonovitch, D. Allara, C. Chang, T. Gmitter, and T. Bright, Unusually Low Surface-Recombination Velocity on Silicon and Germanium Surfaces, *Phys. Rev. Lett.* **57**, 249 (1986).
- [31] D. J. Michalak, F. Gstrein, and N. S. Lewis, The Role of Band Bending in Affecting the Surface Recombination Velocities for Si(111) in Contact with Aqueous Acidic Electrolytes, *J. Physical Chemistry C* **112**, 5911 (2008).
- [32] G. K. Celler, and S. Cristoloveanu, Frontiers of Silicon-on-Insulator, *J. Appl. Physics* **93**, 4955 (2003).
- [33] W. Kern, The Evolution of Silicon-Wafer Cleaning Technology, *Journal of the Electrochemical Society* **137**, 1887 (1990).

- 
- [34] See Supplemental Material at [http://link.aps.org/ supplemental/](http://link.aps.org/supplemental/) for more detailed information on the model we have used here.
- [35] H. J. Ryu, Z. Aksamija, D. M. Paskiewicz, S. A. Scott, M. G. Lagally, I. Knezevic, and M. A. Eriksson, Quantitative Determination of Contributions to the Thermoelectric Power Factor in Si Nanostructures, *Physical Review Letters* **105**, 256601 (2010).
- [36] L. J. van der Pauw, Method of Measuring Specific Resistivity and Hall Effect of Discs of Arbitrary Shape, *Philips Research Reports* **13**, 1 (1958).
- [37] G. Hamaide, F. Allibert, H. Hovel, and S. Cristoloveanu, Impact of Free-Surface Passivation on Silicon on Insulator Buried Interface Properties by Pseudotransistor Characterization, *J. Appl. Physics* **101**, 114513 (2007).
- [38] C. R. Helms, and E. H. Poindexter, The Silicon Silicon-Dioxide System - Its Microstructure and Imperfections, *Reports on Progress in Physics* **57**, 791 (1994).
- [39] Y. Chabal, G. Higashi, K. Raghavachari, and V. Burrows, Infrared-Spectroscopy of Si(111) and Si(100) Surfaces After HF Treatment - Hydrogen Termination and Surface-Morphology, *J. Vacuum Science & Technology A: Vacuum, Surfaces, and Films* **7**, 2104 (1989).
- [40] R. Schlaf, R. Hinogami, M. Fujitani, S. Yae, and Y. Nakato, Fermi Level Pinning on HF Etched Silicon Surfaces Investigated by Photoelectron Spectroscopy, *J. Vacuum Science & Technology A: Vacuum, Surfaces, and Films* **17**, 164 (1999).
- [41] D. Watanabe, A. En, S. Nakamura, M. Suhara, and T. Okumura, Anomalously Large Band-Bending for HF-Treated p-Si Surfaces, *Appl. Surface Science* **216**, 24 (2003).
- [42] H. Angermann, W. Henrion, M. Rebien, and A. Röseler, Wet-chemical Preparation and Spectroscopic Characterization of Si Interfaces, *Appl. surface science* **235**, 322 (2004).

- 
- [43] G. Dubey, G. P. Lopinski, and F. Rosei, Influence of Physisorbed Water on the Conductivity of Hydrogen Terminated Silicon-on-Insulator Surfaces, *Applied Physics Letters* **91**, 232111 (2007).
- [44] K. Sinniah, M. G. Sherman, L. B. Lewis, W. H. Weinberg, J. T. Yates Jr, and K. C. Janda, Hydrogen Desorption from the Monohydride Phase on Si(100), *J. Chemical Physics* **92**, 5700 (1990).
- [45] W. Peng, Electrical Characterization of Silicon Nanomembranes, ProQuest Dissertations and Theses 2013.
- [46] M. Zamiri, S. A. Scott, W. Peng, and M. G. Lagally, in preparation.